ELSEVIER

Journal of Fluids and Structures 23 (2007) 733–753

JOURNAL OF FLUIDS AND STRUCTURES

www.elsevier.com/locate/jfs

Instability of nonlinear standing waves in front of a vertical wall

W. Romańczyk*

Dessau-Soprin Inc., 2 Saint-Germain Est, Bureau 110, Rimouski, QC, Canada G5L 8T7

Received 13 September 2005; accepted 20 October 2006
Available online 23 February 2007

Abstract

The standing waves formed in front of a vertical breakwater in Gdańsk North Port Harbour are examined. To simplify the wave-structure interaction problem, a laboratory experiment and mathematical model were designed. Standing waves in a limited space were generated under resonance conditions between a vertical wall and wave generator. Such slowly growing standing waves eventually become unstable and, consequently, create an impact impulse on the vertical wall. The dynamics of the vertical wall and hydrodynamics of the standing wave were measured and compared with a numerical model derived by variational calculus. The phenomenon of standing wave instability observed in nature was reproduced by laboratory experimentation and numerical simulation. The presented mechanism of breaking standing waves is more complicated in reality due to wave randomness and the multidirectional wave field.

Keywords: Standing waves; Instability; Vertical breakwater; Wave breaking; Vertical accelerations; Numerical modeling

1. Introduction

1.1. General remarks

The main task in the design and exploitation of marine structures is the analysis of interactions between the structure and fluid. Breakwaters are typical structures that protect harbours against sea waves from the surrounding ocean environment. The fundamental aims of breakwaters are energy dissipation and the reflection of water waves. Interactions between structures and waves depend strongly on construction stiffness, foundation method, shape of underwater parts, and so forth. Various designs change the energy of progressive waves to reflected waves, or dissipate their energy on the body of the structure. Others absorb wave energy and then dissipate it inside the structure. The most common marine structure that protects harbours against water waves are monolithic vertical breakwaters.

For the design of a breakwater, the determination of forces exerted on the structure is crucial. In the literature, nonbreaking wave loading on vertical structures is well described, but breaking waves acting on vertical structures are not fully understand. Presently, analytical methods that calculate breaking wave forces do not produce satisfactory solutions. Laboratory experiments and verification of existing structures provide important information needed to

*Tel.: +1 418 723 4010; fax: +1 418 723 4058.
E-mail address: wromanczyk@yahoo.ca.

0889-9746/$ - see front matter
doi:10.1016/j.jfluidstructs.2006.10.013

create adequate mathematical and numerical models. To avoid difficulties with numerical models that are still under development, marine structures are often designed on the basis of regular wave assumptions. The literature contains well-verified calculation schemes [see for example, Bruun, 1986; Dean and Dalrymple, 1984; Goda, 1985; Le Méhauté, 1976; Wiegel, 1964; Coastal Engineering Manual, 2001]. Approximate calculation methods supported by nonbreaking wave theory give significantly varying results, and must be used carefully in engineering practice.

The aim of this paper was to study, through experiments and theory, the interactions between standing waves and vertical walls. One of the vertical wall breakwater sections in Gdańsk North Port Harbour was adopted as a field observation station. Water depth in front of the breakwater was about 12 m, and the slope of the bottom nearby was practically negligible, so that classical, progressive wave breaking was not applicable. Instead, standing waves were often formed during storm waves (average heights $\sim$3 m with wave direction mostly perpendicular to the breakwater wall). The area geometry of the formation of standing waves in front of a breakwater in Gdańsk North Port Harbour has been well described by Hueckel (1976). These extreme standing waves often lose stability and, as a consequence, create a shock impact, causing the vibration of breakwater caissons that was measured by acceleration gauges. The field data do not precisely determine the nature and moment when instantaneous wave forces load the breakwater. The impact could be correlated with water and spray jets thrown upward as well as by jet falling into the wave trough. This phenomenon, observed and measured at the breakwater in Gdańsk North Port Harbour, inspired us to investigate it through laboratory experimentation and mathematical modelling. The hypothesis was that loss of stability of standing waves on the vertical wall was acting as a dominant cause that brought this heavy breakwater caisson to vibration, and impact accelerations were mostly caused by the fluid descending the wall and hitting the rest of the water domain.

To understand the mechanism of loss of stability of standing waves in front of a vertical structure, a laboratory model was built. The physical model, composed of a rigid vertical plate supported elastically at the bottom (see Fig. 1), simplified the breakwater caisson. The vertical plate was kept in an equilibrium state by a system of springs, with the possibility of free pivoting at the lowest edge on the bed, mapping the first mode of free vibration of the breakwater caisson in Gdańsk North Port Harbour (see Section 2.2). To simulate the moment when the standing waves lost their stability, the vertical plate was loaded by standing waves of regular sinusoidal form growing to an extremely nonlinear shape that, in the end, led to wave instability. Measurement of plate dynamics (acceleration at the top) showed precisely the moment when the standing waves broke and loaded the plate by instantaneous impact.

A system of pressure gauges fixed in front of the experimental plate and a wave metre were installed to investigate changes in the hydrodynamic field and used for comparison with a mathematical model. The mathematical model of growing standing waves presented hereafter was formulated by an Eulerian description assuming a perfect fluid. Euler's equations were not solved. Instead, a variational principle (consistent with Euler's equations for incompressible, irrotational fluid motion) served to obtain time-dependent coefficients of suitable expressions for unknown field variables.

1.2. Existing models

The literature concerning hydrodynamic loads on a vertical breakwater can be sorted into three groups. The first group describes standing waves and interactions between regular water waves and vertical structures. The second group offers criteria for standing wave instability, and the third relates to analysis of forces on vertical structures.

The main problem addressed is to describe the hydrodynamic loads on vertical breakwaters. A basic method for calculating hydrodynamic pressures was proposed by Sainflou (1928). However, it gives values of the forces on the wall which are too high when wave steepness is large. The most popular calculating technique is that of Rundgren (1958), supported by Miche's theory (1944). It is recommended in the Coastal Engineering Manual (2001) for the practical assessment of standing wave forces. Standing waves in water of infinite depth were first considered by Lord Rayleigh (1915), who calculated a perturbation series based on wave amplitude to the third order. Penney and Price (1952) generalized this perturbation series approach to the fifth order. Tadjbakhsh and Keller (1960) calculated a third-order perturbation series for finite depth standing waves. This was enlarged by Goda (1967), who extended the perturbation series to the fourth order. All the above-mentioned solutions of nonlinear standing waves were carried out in Euler coordinates. In contrast, Lappo and Zagryadskaya (1977) developed a third-order solution in Lagrange coordinates. The perturbation solution satisfying the uniqueness condition was given by Vanden-Broeck (1984), and approximation to the third order, using wave height as a perturbation parameter, was undertaken by Fenton (1985).

All the above-mentioned solutions have analytical mathematical forms. To extend the order of approximation, Schwartz and Whitney (1981) undertook a conformal mapping to simplify the perturbation series and calculated it numerically to the 25th order; this expansion was later validated by Amick and Toland (1987). More recent studies of

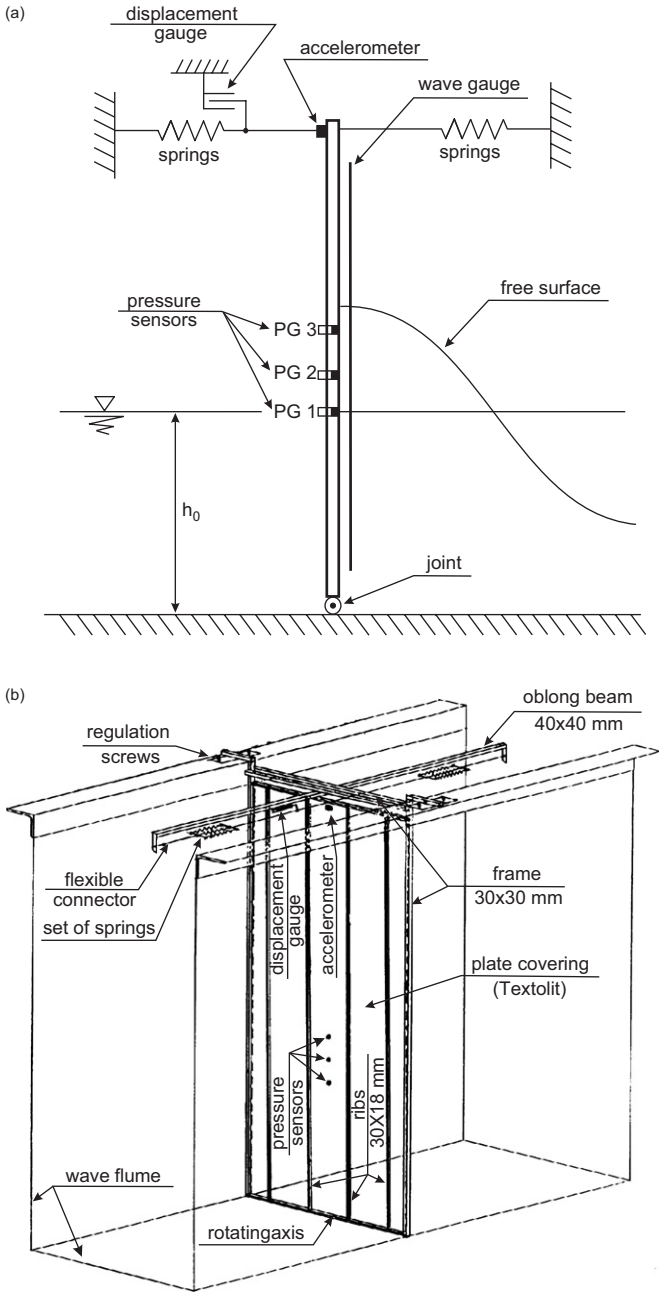

Fig. 1. Schematics of the experimental set-up: (a) as a dynamic system, (b) as a technical 3-D sketch.

standing water waves include those of Mercer and Roberts (1992, 1994), Tsai and Jeng (1994), Schultz et al. (1998) and Jeng (2002). There is also much recent activity concerned with standing waves making jets (Longuet-Higgins, 2001, 2002), but much has yet to be learned about jet formation.

Besides mathematical models, experimental investigations of regular waves near a vertical wall were carried out by Fultz (1962), Nagai (1968, 1969) and Iwagaki et al. (1980). They belong to the conventional first group as well.

The second group describes a limiting form (steepness) of the gravity standing wave before breaking. Theoretical work on stability criteria has been presented by Kishi (1959), and Penney and Price (1952), whereas Miche (1944), Danel (1952), Iwata and Kiyono (1985) proposed semi-empirical solutions. Experimental investigations were pursued

by Goda (1972), demonstrating the transition from nonbreaking to post-breaking shapes of wave pressures in front of a vertical wall.

The literature describing the impulse of shock pressures of breaking waves acting on a vertical wall belongs to the third group of classification, and is very rich. Analytical descriptions of this phenomenon do not exist. Only semi-empirical formulas and approximate mathematical models have been developed. The compendium of works dating up to 1974 is well documented by Richert (1974). Solutions obtained by numerical simulation are presented by Vinje and Brevig (1981) and Cooker and Peregrine (1990a, b, 1992, 1995). Wood and Peregrine (1998) describe the results of pressure–impulse modelling of three-dimensional (3-D) wave impacts, and pressure–impulse distribution was developed by these same authors (Wood and Peregrine, 2000). Classification of breaking wave forces on vertical structures was done, among others, by Lundgren (1969), Kjeldsen (1981), and Oumeraci et al. (1992, 1993, 2001).

The brief review of existent publications shows scientific endeavours to explain and understand the impact of water waves on the vertical structures. This paper focuses on the phenomenon of nonlinear standing waves and their loss of stability that leads to an instantaneous force impulse acting on the vertical wall.

2. Experiments

2.1. Field measurements at the breakwater in Gdańsk North Port Harbour

A section of the breakwater in Gdańsk North Port Harbour was instrumented to measure horizontal accelerations at two points on top of the caisson, pressures at four points under the mean water level, and surface elevation at three points on the seaward side of the breakwater. A detailed description of the Marine Harbour Laboratory were given by Sobierajski (1992) and Romańczyk and Sobierajski (1994). Water depth in front of the breakwater is of sufficient depth, and the slope of the bottom is practically negligible, so that classical, progressive wave breaking is not applicable. Therefore, in Gdańsk North Port Harbour, the loss of stability of water waves is observed on the intermediate water depth in front of the vertical wall (Hueckel, 1976; Romańczyk and Sobierajski, 1994). An example of water surface elevation and simultaneous acceleration at the top of the caisson are presented in Fig. 2. The frequency of the acceleration is several times higher than the observed wave motion. Using a modified Kalman filter procedure (Romańczyk, 1992a, b, 1994), the measured acceleration was decomposed on the fundamental frequency (component 1) associated with the water waves and free vibration of the breakwater caisson (component 2). Analysis determined that free vibrations of the caisson were random and occurred at the wave crest, but the precise time when the shock force was imposed was impossible to detect. The acting forces causing this heavy caisson, weighing about 6.6×10^4 kN, to vibrate were substantial. To understand this phenomenon, a wave flume experiment was performed.

2.2. Wave flume experiment

2.2.1. Equipment

This experiment was undertaken in a laboratory channel 0.90 m wide, 1.3 m high and 25 m long at the Hydroengineering Institute in Gdańsk. A rigid vertical plate, with the pivot at its lowest edge on the bed, and held in equilibrium state by a system of springs mounted at the top of the plate, was constructed to model a vertical breakwater. Such a model has the first free vibration mode similar to the caisson at Gdańsk North Port Harbour (rotation around the axis lying below the breakwater foundation). The experimental set-up is shown in Fig. 1. The experimental model could be located at various positions inside the wave flume that allowed the use of different resonance wavelengths in the experiment. Water tightness on each side of the wave flume was obtained by elastic sealing. The vertical plate was constructed as a steel frame enforced by a system of several beams of 30×30-mm dimension. The front of the steel grate was covered by a smooth 0.45×1.2-m Texstolit plate. The plate was constructed for dynamic scale similarity with real conditions at North Port. The ratio between the first harmonics of the average storm conditions and free vibration of the caisson was about 8. This value for the laboratory model oscillated between 16 and 23. Three pressure transducers were mounted in the central vertical line of the plate. The PG1 gauge was placed at the free-water level. The PG2 and PG3 gauges were 0.1 and 0.2 m adequately above the free-water level. Horizontal deflection of the top of the plate was measured by a displacement transducer, and inertia forces caused by short-lasting shock impulses were recorded by an acceleration gauge, also fixed at the top of the plate. The measurement system was composed of pressure, displacement and acceleration transducers, a system of filters, an analog-digital 12-bit converter, and a data acquisition computer to record the data. Considering the preliminary tests conducted to determine the optimal sampling frequency that would be sufficient to cover the observed physical parameters (wave pressure and

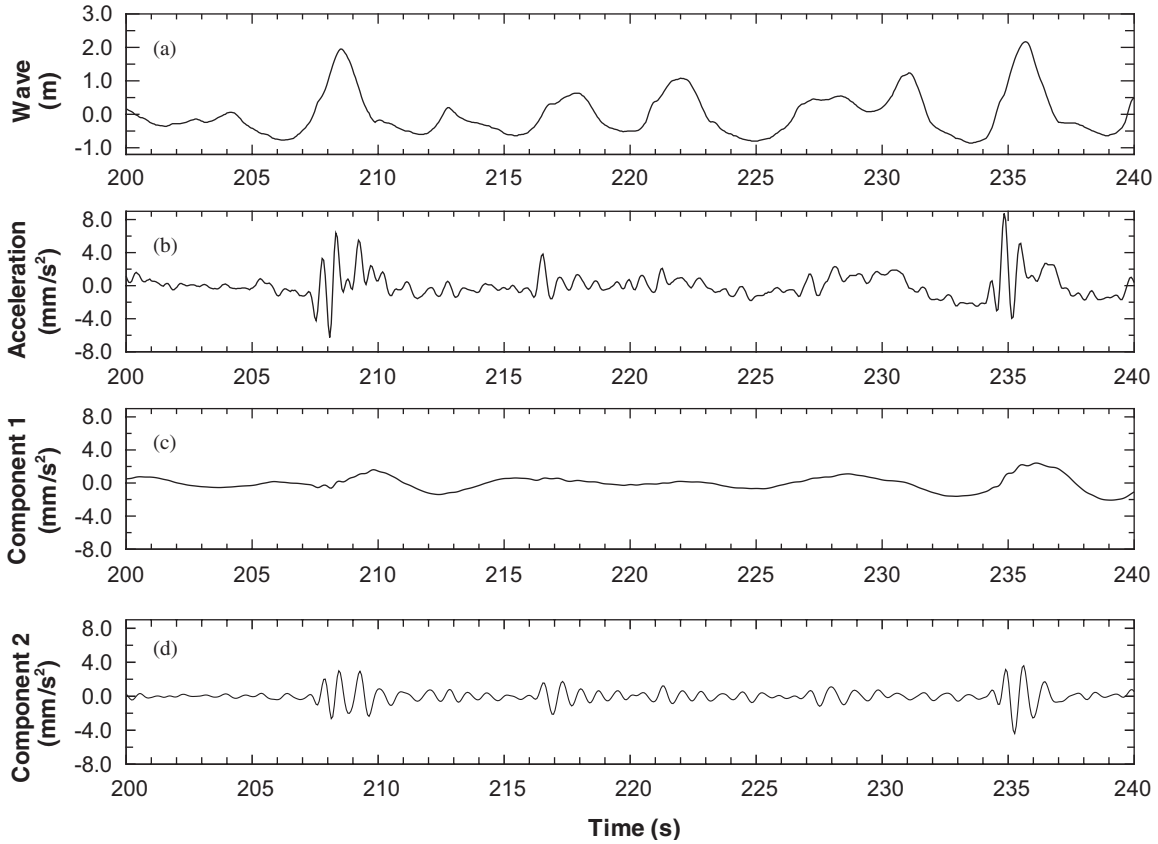

Fig. 2. Measurements of waves and decomposition of measured accelerations using the modified Kalman filter: (a) wave elevation in front of the breakwater; (b) acceleration of the top of the caisson; (c) component associated with the water waves; and (d) with the free vibration of the caisson.

acceleration), the 400 Hz sampling frequency was chosen. The number of sampling points for each run was 4096. For longer recording times, 300 Hz sampling frequency increased the number of sampled points to 15 000 in some experiments.

2.2.2. Procedure

To obtain growing standing waves, the following procedure was established. The vertical wall model was placed in the wave flume at the half wavelength distance from the wave generator to create a resonance condition. To fulfil this assumption, the period of sinusoidal oscillation of a wave generator was calculated for each location of the vertical plate. The wave generator had a small, constant amplitude (about 0.01 m) for each run of the experiment to produce a smooth and slow-wave process. Due to the resonance condition, with every cycle of the wave generator, the height of the standing wave was increased. When wave steepness attained the critical value on the vertical wall, the continuity of the wave surface was broken, and the wall was loaded by impact force. This significant, short-lasting force initiated free vibration of the plate, which was recorded by the displacement and acceleration transducers. The experimental wave parameters, including wave period T, wavelength λ, distance $x = \lambda/2$ between the vertical wall and the wave generator paddle, amplitude A of the wave generator and initial water depth h_0, are presented in Table 1.

A preliminary experiment was carried out for distance x greater than $\lambda/2$, say 4λ to 12λ. As the waves grew in amplitude, the standing waves initially behaved like that at the half-wave distance, but when wave steepness approached the limit, breaking usually appeared in the middle of the wave flume and not at the experimental wall. This led to wave propagation with different phase speeds, and created irregular waves in the flume. Of course, in the end, the wave broke on the wall, causing its vibration, but the process was not as clear as with $x = \lambda/2$ distance. Therefore, further analysis was carried out for the half-wave distance between the wave generator and the vertical wall.

Table 1
Experimental wave parameters for distance $x = \lambda/2$ between a vertical wall and a wave generator paddle

No.	h_0 (m)	T (s)	A (m)	λ (m)	x (m)
1	0.5	1.31	0.011	2.24	1.12
2	0.5	1.38	0.012	2.44	1.22
3	0.5	1.46	0.014	2.64	1.32
4	0.5	1.55	0.015	2.82	1.41
5	0.5	1.58	0.016	3.02	1.51
6	0.5	1.69	0.016	3.24	1.62
7	0.5	1.78	0.019	3.48	1.74
8	0.5	1.84	0.019	3.76	1.88

2.2.3. Experimental data

Typical data obtained from the experiment are presented in Fig. 3, including displacement (positive values indicate direction away from the fluid) and acceleration (positive values indicate direction towards the fluid) at the top of the plate, wave surface elevation near the wall, and pressures at three points on the vertical axis of symmetry. The pressures in the initial stage (see gauges PG1, PG2, and PG3) had a frequency similar to that of the wave. This means that inertia forces have secondary importance, and wave loadings are quasistatic. Pressures evolved over the experiment. At the beginning, only a single peak was seen. Then, after a time lapse, double hump peaks were formed, indicating the growing significance of the harmonics components of standing waves. Finally, when the wave lost its stability, the second hump of the peaks disappeared. This means that some part of the water breaks away at the wave crest. Simultaneously, in the acceleration diagram, the amplitude of free vibrations increased substantially, and showed that the vertical plate was loaded by impulse force (see Fig. 3). The wave gauge revealed that the moment the impulse force appeared was when surface elevation reached the still water level. All tests were recorded by video camera to visualize the experiments.

A sequence of pictures from one run of the experiment (Fig. 4) illustrates the transformation from nonbreaking to breaking waves at the vertical wall. Each photograph was taken at the time of maximum run-up of particular waves. Fig. 4(a) represents the typical profile of a linear standing wave. In Figs. 4(b) and (c), the wave crest becomes more steep, and minor disturbances of stability are evident from local foam on the surface. The first sign of nonlinearity is represented by a small crest formed at about 1/2 length of the resonance distance from the wall (see Fig. 4(d)). Fig. 4(e) shows explicitly how some volume of water is torn away, and immediately falls down toward the decreasing surface water (Fig. 4(f)), creating a shock impulse recorded by the acceleration gauge mounted on the vertical wall.

3. Mathematical model

3.1. Governing equations

The mathematical and numerical model was developed to simulate growing standing waves forced by the sinusoidal movement of a wave generator.

Classical assumptions for the hydrodynamics of a gravitational wave are imposed. The fluid is assumed to be inviscid, incompressible, and the flow irrotational. In the study, a local moving Cartesian coordinate (x, y) was chosen, with the origin taken at the bottom of the moving vertical paddle of a wave generator (see scheme in Fig. 5); the x coordinate is along the bottom, directed to the fixed vertical wall; and the y coordinate is vertically upwards. Therefore, the fluid is bounded on one side by a fixed vertical wall, and on the another side, by the moving vertical paddle of a wave generator, and by the free surface elevation $y = h(x,t)$. Generally, the problem is formulated by variational calculus, then digitized in time, and presented as a nonlinear set of equations to be solved numerically. It is convenient to transform all governing equations and boundary conditions into dimensionless form with reference length k^{-1} and reference time $(gk)^{-1/2}$, in which $k = 2\pi/\lambda$ is the wavenumber λ, is the wavelength and g is the acceleration due to gravity. Then, dimensionless quantities are introduced by

$$(x^*, y^*, h^*) = k(x, y, h), \quad \phi^* = \frac{k^2}{\sqrt{gk}}\varphi, \quad t^* = \omega t, \ \omega^* = \frac{1}{\sqrt{gk}}\omega, \tag{1}$$

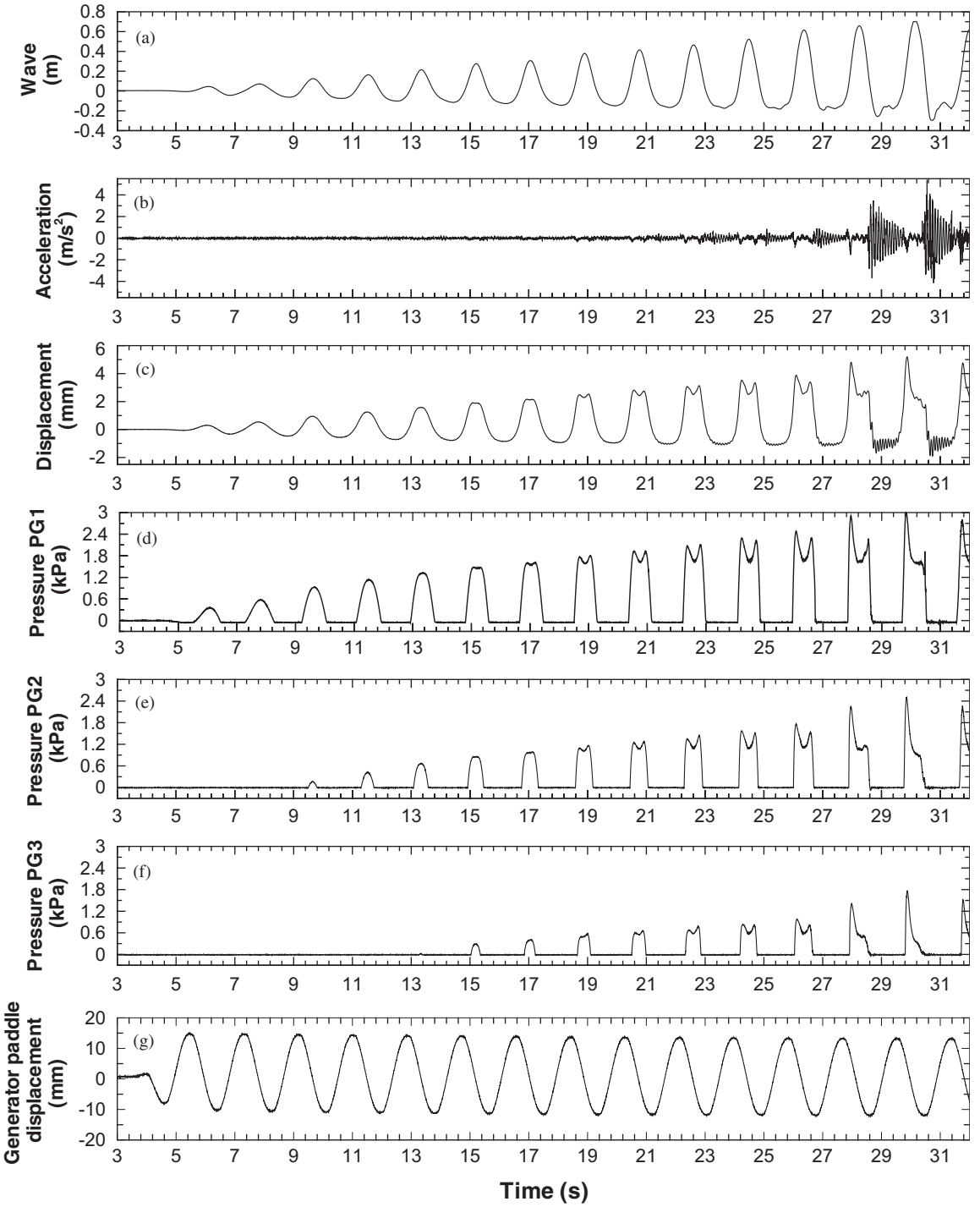

Fig. 3. Experimental data for wave period $T = 1.84$ s, and wave length $\lambda = 3.76$ m: (a) wave elevation on vertical plate, (b) acceleration and (c) displacement at the top of the vertical plate; pressure in the fluid on vertical plate at (d) 0.5 m, (e) 0.6 m, and (f) 0.7 m level, (g) displacement of the wave generator paddle.

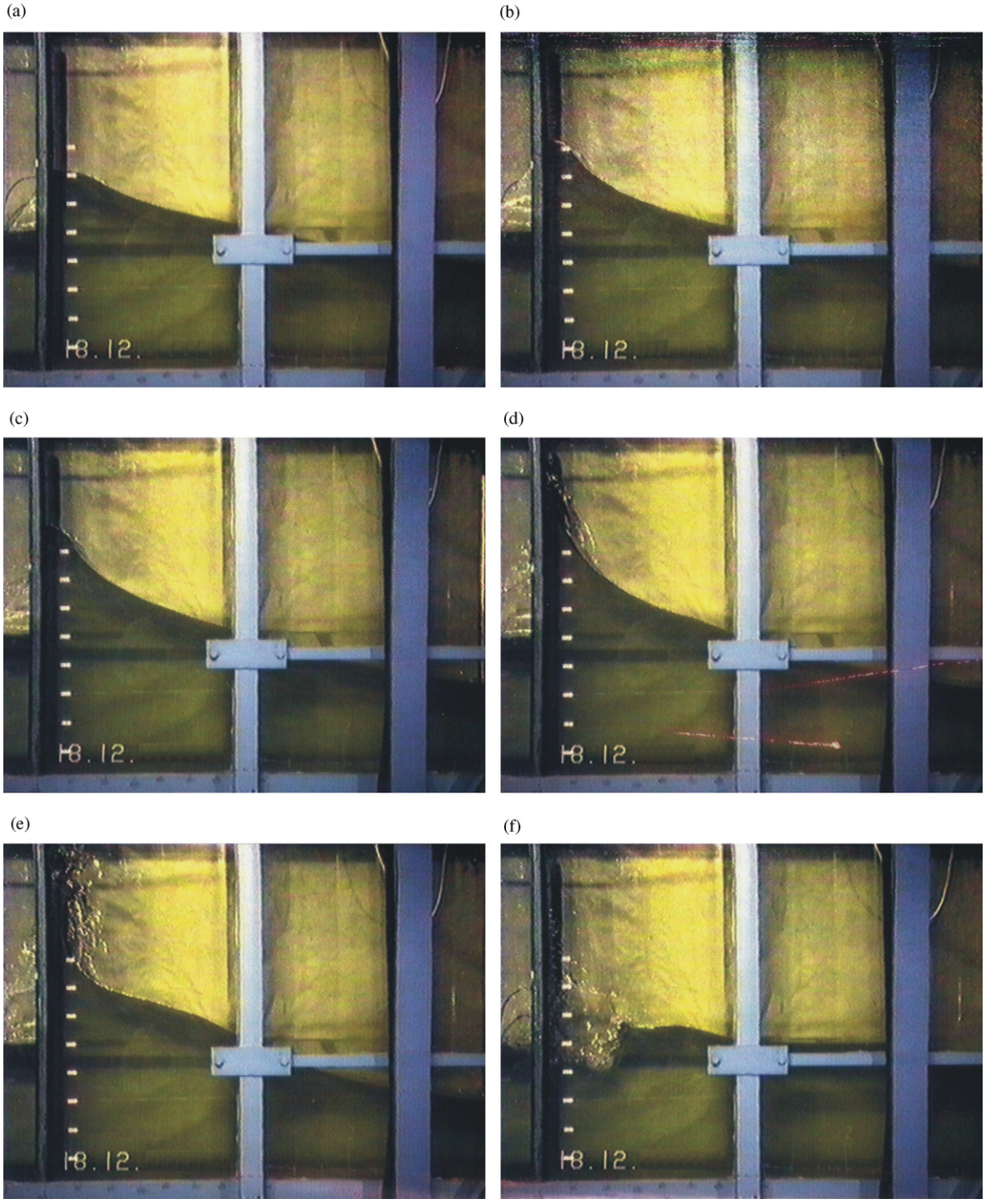

Fig. 4. Sequence of pictures from (a) to (f) showing the process of loss of stability of the wave with period $T = 1.78$ s and length $\lambda = 3.48$ m. The photographs were taken at the following time steps: (a) 14.24 s, (b) 16.02 s, (c) 17.8 s, (d) 19.58 s, (e) 21.36 s, and (f) 21.65 s, counting from the beginning of the experiment.

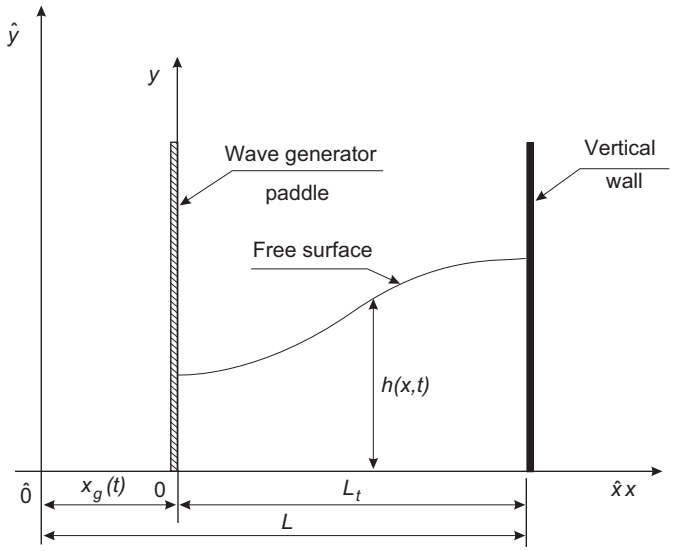

Fig. 5. Scheme of the analysed system in global $\hat{0}\hat{x}\hat{y}$ and local moving coordinates $0xy$.

where $\omega = 2\pi/T$ is the wave frequency, and t the time. The asterisks (*) denoting dimensionless quantities will be omitted in what follows for the sake of simplicity. The velocity potential ϕ, defined in the local moving coordinate system Oxy for the considered space, is described by the sum:

$$\phi(x, y, t) = \phi_0(x, y, t) + \phi_s(x, y, t). \tag{2}$$

The first part of Eq. (2) is represented by the polynomial

$$\phi_0(x, y, t) = \dot{x}_g(t)\left[x - \frac{1}{2L_t}(x^2 - y^2)\right], \tag{3}$$

where $L_t = L - x_g(t)$ and $L = \lambda/2$ is half of wavelength, $x_g(t) = -A\cos(\omega t)$ is the displacement of the paddle of the wave generator, and $\dot{x}_g(t)$ its velocity. The second part of potential function ϕ and free surface elevation is described by cosine series:

$$\phi_s(x, y, t) = b_0(t) + \sum_{n=1}^{\infty} b_n(t)\cosh\left(\frac{n\pi y}{L_t}\right)\cos\left(\frac{n\pi x}{L_t}\right), \tag{4}$$

$$h(x, t) = h_0 + c_0(t) + \sum_{n=1}^{\infty} c_n(t)\cos\left(\frac{n\pi x}{L_t}\right), \tag{5}$$

where h_0 is the water depth. The functions $b_0(t)$, $b_n(t)$, $c_0(t)$ and $c_n(t)$ in Eqs. (4) and (5) are unknown coefficients. The potential function in Eq. (2) fulfils boundary conditions on both sides of the space and on the bottom. To satisfy dynamic and kinematic conditions on the free surface, the coefficients $b_0(t)$, $b_n(t)$, $c_0(t)$ and $c_n(t)$ have to be chosen properly. A direct method that calculates unknown coefficients does not exist because they are involved both in the free surface and boundary conditions. One of the methods that minimizes the expression of certain functions is variational calculus, and it is used here. The existence of a Lagrangian for irrotational free surface flows was introduced originally by Luke (1967), who showed that the Lagrangian was given by the integral of fluid pressure over depth, i.e.,

$$L_g = \rho \int_0^{h(x,t)} \left(\tfrac{1}{2}\phi_{,x}^2 + \tfrac{1}{2}\phi_{,y}^2 + \omega\phi_{,t} + y\right) \mathrm{d}y, \tag{6}$$

where ρ is the fluid density. Luke's principle states that the integral of L_g over all horizontal space and time is then stationary with respect to variations in h and ϕ:

$$\delta J = \int_{t_1}^{t^2} \int_{x_1}^{x_2} L_g \,\mathrm{d}x\,\mathrm{d}t = 0, \tag{7}$$

where we neglected the influence of lateral boundaries in the specification of the problem. An examination of Eq. (6) shows that the integrand consists of the difference of the kinetic energy E_k and the potential energy E_p. Then Eq. (6) is fully equivalent to the usual Lagrangian form from classical mechanics:

$$L_g = E_k - E_p. \tag{8}$$

It is noteworthy to say that the natural boundary conditions obtained from functional (6) by variational calculus are adequate for classical boundary conditions in water wave theory. The method implemented for the area with one moving boundary (see Fig. 5) leads to the following functional form:

$$J = \rho \int_{t_1}^{t_2} \int_0^{L_t} \int_0^{h(x,t)} \left[\frac{1}{2}(\phi_{0,x} + \phi_{s,x})^2 + \frac{1}{2}(\phi_{0,y} + \phi_{s,y})^2 - \dot{x}_g(t)(\phi_{0,x} + \phi_{s,x}) + \omega(\phi_{0,t} + \phi_{s,t}) + y \right] \mathrm{d}x\,\mathrm{d}y\,\mathrm{d}t. \tag{9}$$

Variational calculus of the above functional gives the Laplace equation:

$$\nabla^2(\phi_0 + \phi_s) = 0 \quad \text{for} \quad 0 < y < h(x,t), \quad 0 < x < L_t, \tag{10}$$

and natural boundary conditions:

(i) dynamic free surface boundary for $y = h(x,t)$, $0 < x < L_t$:

$$\frac{1}{2}(\phi_{0,x} + \phi_{s,x})^2 + \frac{1}{2}(\phi_{0,y} + \phi_{s,y})^2 - \dot{x}_g(t)(\phi_{0,x} + \phi_{s,x}) + \omega(\phi_{0,t} + \phi_{s,t}) + y = 0; \tag{11}$$

(ii) kinematic free surface boundary for $y = h(x,t)$, $0 < x < L_t$:

$$-h_{,x}(\phi_{0,x} + \phi_{s,x}) + \phi_{0,y} + \phi_{s,y} - \omega h_{,t} + \omega h_{,x}\dot{x}_g(t) = 0; \tag{12}$$

(iii) bottom boundary for $y = 0$, $0 < x < L_t$:

$$-(\phi_{0,y} + \phi_{s,y}) = 0; \tag{13}$$

(iv) moving wall boundary (generator) for $x = 0$, $0 < y < h(x,t)$:

$$\dot{x}_g(t) - (\phi_{0,x} + \phi_{s,x}) = 0; \tag{14}$$

immovable wall boundary for $x = L_t$, $0 < y < h(x,t)$:

$$\phi_{0,x} + \phi_{s,x} = 0. \tag{15}$$

The same formalism was performed for functions ϕ and h represented by series (Eqs. (4) and (5)). The solution, parameterized by the new variational variables $b_0(t)$, $b_k(t)$ ($k = 1,2,\ldots$) and $c_0(t)$, $c_k(t)$ ($k = 1,2,\ldots$), leads to the same natural conditions and the Laplace equation for any kth components just described above. This indicates that functional (9) and potential function (2) fulfil all boundary conditions for the assumed fluid area. The above problem is presented in a $0xy$, local moving coordinate system. Transformation to the global coordinate system $\hat{0}\hat{x}\hat{y}$ (see Fig. 5) involves the following equations:

$$\hat{x} = x + x_g(t), \quad \hat{L} = L_t + x_g(t), \quad \hat{y} = y, \quad \hat{t} = t. \tag{16}$$

3.2. Numerical procedure

The problem of nonlinear standing waves described in Section 3.1 is well described in space. To solve the problem numerically in time, the derivatives are discretized by forward difference, and the values of functions are calculated in the middle of the discretization points. This leads to the following discrete form for functional (9):

$$J = \rho\,\Delta t \sum_{k=1}^{N} \int_0^{L_{t2}(r+1,r)} \int_0^{y_{t2}(r+1,r)} F(x,\ y,\ r,\ r+1,\ b_0,\ b_1,\ \ldots,\ b_n,\ c_0,\ c_1,\ \ldots,\ c_n)\,\mathrm{d}x\,\mathrm{d}y, \tag{17}$$

where function F is defined in Appendix A, Δt indicates the time step, r is a time counter ($r\Delta t$), N is the number of coefficients used in the discretization, y is the free surface elevation, and L_{t2} is the moving distance between a wave

generator paddle and the vertical wall as described below:

$$y_{t2}(r+1,r) = h_0 + \frac{c_0(r+1)+c_0(r)}{2} + \sum_{n=1}^{N} \frac{c_n(r+1)+c_n(r)}{2} \cos\left(\frac{n\pi x}{L_{t2}(r+1,r)}\right),$$
$$L_{t2}(r+1,r) = \frac{L_t(r+1)+L_t(r)}{2}. \tag{18}$$

Solutions to the problem above, posed in a finite fluid domain, can be obtained from the extremum of functional (17). Integrating analytically with respect to y and using variational calculus with respect to variables b_0, $b_k(t)$ ($k = 1,2, \ldots, N$) and c_0, $c_k(t)$ ($k = 1,2, \ldots, N$) lead to two recurrence equations:

(i)
$$c_0(r+1) = c_0(r)\frac{x_g(r+1)-x_g(r-1)}{2L-x_g(r)-x_g(r+1)} + c_0(r-1)\frac{2L-x_g(r-1)-x_g(r)}{2L-x_g(r)-x_g(r+1)}, \tag{19}$$

(ii)
$$b_0(r+1) = b_0(r)\frac{L_t(r+1)-L(r-1)}{L_t(r)+L_t(r+1)} + b_0(r-1)\frac{L_t(r-1)-L_t(r)}{L_t(r)-L_t(r+1)} - \frac{2\Delta t}{\omega(L_t(r)+L_t(r+1))} \times \left[\begin{array}{l} \int_0^{L_{t2}(r+1,r)} F_1(x, r+1, r, b_1, \ldots, b_n, c_0, c_1, \ldots, c_n)\,\mathrm{d}x \\ + \int_0^{L_{t2}(r,r-1)} F_1(x, r+1, r, b_1, \ldots, b_n, c_0, c_1, \ldots, c_n)\,\mathrm{d}x \end{array}\right], \tag{20}$$

and a nonlinear system of k equations where $k = 1,2,\ldots,N$:

(iii)
$$\int_0^{L_{t2}(r+1,r)} F_1(x,\ r+1,\ r, b_1, \ldots b_n, c_0, c_1, \ldots, c_n)\cos\left(\frac{k\pi x}{L_{t2}(r+1,r)}\right)\mathrm{d}x + \int_0^{L_{t2}(r,r-1)} F_1(x,\ r,\ r-1,\ b_1, \ldots, b_n, c_0, c_1, \ldots, c_n)\cos\left(\frac{k\pi x}{L_{t2}(r,r-1)}\right)\mathrm{d}x = 0, \tag{21}$$

(iv)
$$\left\{\begin{array}{l} \text{when the } n\text{th element in series summation is } n \neq k \\ \int_0^{L_{t2}(r+1,r)} F_2(x,k,r+1,r,b_1,\ldots,b_n,c_0,c_1,\ldots,c_n,-1)\,\mathrm{d}x \\ + \int_0^{L_{t2}(r,r-1)} F_2(x,k,r,r-1,b_1,\ldots,b_n,c_0,\ c_1,\ldots,c_n,1)\,\mathrm{d}x \\ \text{and when the } n\text{th element in series summation is } n = k \\ + \int_0^{L_{t2}(r+1,r)} F_3(x,\ k,\ r+1,r,\ b_1,\ldots,b_n,\ c_0,\ c_1,\ldots,c_n)\,\mathrm{d}x \\ + \int_0^{L_{t2}(r,r-1)} F_3(x,\ k,\ r,\ r-1,\ b_1,\ldots,b_n,c_0,c_1,\ldots,c_n)\,\mathrm{d}x = 0, \end{array}\right. \tag{22}$$

where functions $F_1(\cdots)$, $F_2(\cdots)$ and $F_{3d}(\cdots)$ are given in Appendix A. The system of equations presented above completely describes a standing wave problem while considering areas forced by the moving wave paddle. The unknown coefficients b_0, c_0, b_n, c_n in time $r+1$ are dependent on two preceding time steps r and $r-1$ and have to be solved numerically. The initial coefficients for time $r = 0$ and $r = 1$ can be calculated from a linear version of the analysed problem. Assuming linear wave theory and displacements of the wave generator, substantially small in comparison to horizontal distance ($L_t = L$), leads to a linear system of equations with respect to the continuous variable t:

(i)
$$\ddot{x}_g(t)\left[\frac{L^2}{3}+\frac{h_0^2}{2}\right]\omega^2 + b_{0,t}(t)L\omega + L(h_0 + c_0(t)) = 0, \tag{23}$$

(ii)
$$-c_0(t)L\omega + \ddot{x}_g(t)h_0\omega = 0, \tag{24}$$

(iii)
$$-\ddot{x}_g(t)\left(\frac{L}{k\pi}\right)^2\omega^2 + \frac{1}{2}b_{k,t}(t)\cosh\left(\frac{k\pi h_0}{L}\right)L\omega + \frac{1}{2}c_k(t)L = 0, \tag{25}$$

(iv)
$$\frac{1}{2}b_k(t)\left(\frac{k\pi}{L}\right)\sinh\left(\frac{k\pi h_0}{L}\right)\cosh\left(\frac{k\pi h_0}{L}\right)L - \frac{1}{2}c_{k,t}(t)\cosh\left(\frac{k\pi h_0}{L}\right)L\omega = 0, \tag{26}$$

that are the linear equivalent of Eqs. (19)–(22). The above linear system of equations has an analytical solution of variables b_0, $b_k(t)$ ($k = 1,2, \ldots, N$) and c_0, $c_k(t)$ ($k = 1,2, \ldots, N$) at any time t and can serve as a solution for the first two

time steps ($r=0$ and 1). Eqs. (21) and (22) form a conjugate nonlinear system that has to be solved first to obtain $b_1, \ldots, b_n$ and $c_1, \ldots, c_n$ coefficients for time $r+1$, and then the coefficients b_0 and c_0 can be calculated from recurrence Eqs. (19) and (20). The classical Broyden (1965) method was applied to solve numerically this nonlinear system of equations (Eqs. (21) and (22)). The proposed method is well known in the literature (Press et al., 1992), and in our case is relatively fast, owing to the Jacobian matrix calculated only once at each time step. At the end of the calculation, the following norm of convergence is applied at each time step:

$$\frac{\sqrt{f_1^2+f_1^2+\cdots+f_N^2}}{N}<\delta_E, \tag{27}$$

where δ_E is the convergence limit, and $f_1^2, f_2^2, \ldots, f_N^2$ are function residual values of each of N equations in the nonlinear system. Simulation of the experiment was completed when the maximum number of iterations $i_{\max}$ in a single time step did not satisfy the norm of convergence (27). In the simulations performed, the following norms are used: $i_{\max}=100$ and $\delta_E=10^{-10}$.

Functions $F_1(\ldots)$, $F_2(\ldots)$ and $F_3(\ldots)$ include hyperbolic functions that have as argument a multiplication of series. To conform with the assumed order of solutions in the numerical scheme, the hyperbolic functions were expanded into Taylor series, and only terms with an exponent not larger than the assumed order were kept as solutions. The integrals on the horizontal dimension x in Eqs. (20)–(22) are calculated numerically by the standard Romberg adaptive method (Press et al., 1992).

The proposed numerical scheme describes the development of growing standing waves forced by the sinusoidal movement of a wave generator paddle in a time domain from still water to the moment where the wave is close to breaking. Knowing the water depth h_0, standing wave length L, amplitude of wave generator A, and assumed time step Δt, the development of free surface elevations, velocity and pressure field in the fluid during the lapse of time base on coefficients b_0, c_0, b_n, c_n is obtained by solution of the system of Eqs. (19)–(22) at each time step. The simulation stops when the convergence criterion (27) is not satisfied for the maximum number of iterations $i_{\max}$.

3.3. Accuracy

The discrete linear version of the full system of Eqs. (19)–(22) can be obtained by neglecting nonlinear terms and using the approximations: $L_{t2}(r+1, r)=L$, $L_{t2}(r, r-1)=L$, and $y_{t2}(r, r-1)=h_0$. Finally, the discrete linear system of equations has the following form:

(i)
$$\frac{x_g(r+2)-2x_g(r)+x_g(r-2)}{4\Delta t^2}\left(\frac{L^2}{3}+\frac{h_0^2}{2}\right)\omega^2+\frac{b_0(r+1)-b_0(r-1)}{2\Delta t}\times L\omega+L\left(h_0+\frac{c_0(r+1)+2c_0(r)+c_0(r-1)}{4}\right)=0, \tag{28}$$

(ii)
$$-\frac{c_0(r+1)-c_0(r-1)}{4\Delta t}2L\omega+\frac{x_g(r+1)-x_g(r-1)}{2\Delta t}h_0\omega=0, \tag{29}$$

(iii)
$$-\frac{x_g(r+2)-2x_g(r)+x_g(r-2)}{4\Delta t^2}\left(\frac{L}{k\pi}\right)^2\omega^2+\frac{b_k(r+1)-b_k(r-1)}{4\Delta t}\times\cosh\left(\frac{k\pi h_0}{L}\right)L\omega+\frac{c_k(r+1)+2c_k(r)+c_k(r-1)}{8}L=0, \tag{30}$$

(iv)
$$\frac{b_k(r+1)+2b_k(r)+b_k(r-1)}{8}\left(\frac{k\pi}{L}\right)\sinh\left(\frac{k\pi h_0}{L}\right)\cosh\left(\frac{k\pi h_0}{L}\right)L-\frac{c_k(r+1)-c_k(r-1)}{4\Delta t}\cosh\left(\frac{k\pi h_0}{L}\right)L\omega=0. \tag{31}$$

The above discrete linear system of equations can be solved for any discrete time step r. Both linear systems in the continuous (Eqs. (23)–(26)) and in the discrete scheme (Eqs. (28)–(31)) were used to check the influence of disretisation on the results. Comparison between discrete and analytical solutions clarifies how numerical errors are propagated by the assumed numerical algorithm. For the chosen time step Δt, the error function in a time domain was calculated by

the following formula:

$$\delta_{\Delta t}(t) = \frac{\sqrt{\sum_1^n \Delta b_n^2(t) + \sum_1^n \Delta c_n^2(t)}}{\sqrt{\sum_1^n b_{n,c}^2(t) + \sum_1^n b_{n,d}^2(t)}}, \tag{32}$$

where $\Delta b_n = b_{n,c} - b_{n,d}$ and $\Delta c_n = c_{n,c} - c_{n,d}$. The coefficients $b_{n,d}$ and $c_{n,d}$ were obtained from numerical calculations, and $b_{n,c}$, $c_{n,c}$ from analytical forms of equations. The error function (32) between the discrete and analytical solutions in percentage are shown in Fig. 6(a) for the following parameters: time step $\Delta t = 0.01$ s, waterdepth $h_0 = 0.5$ m, wavelength $\lambda = 2.82$ m, and wave generator amplitude $A = 0.02$ m. For all sets of initial parameters (wavelength, amplitude, etc.) used in the laboratory experiment, the maximum calculated error (32) was 1.35%. It is noteworthy that the maximum recording time in our experiment did not exceed 35 s. Error propagation (calculated for $t = 100$ s) as a function of model time step Δt varying from 0.0001 to 0.1 s are presented in Fig. 6(b). The errors propagated by numerical scheme increase up to time step $\Delta t = 0.07$ s, and then stabilize at the value of 1.8%. Analysis of the linear

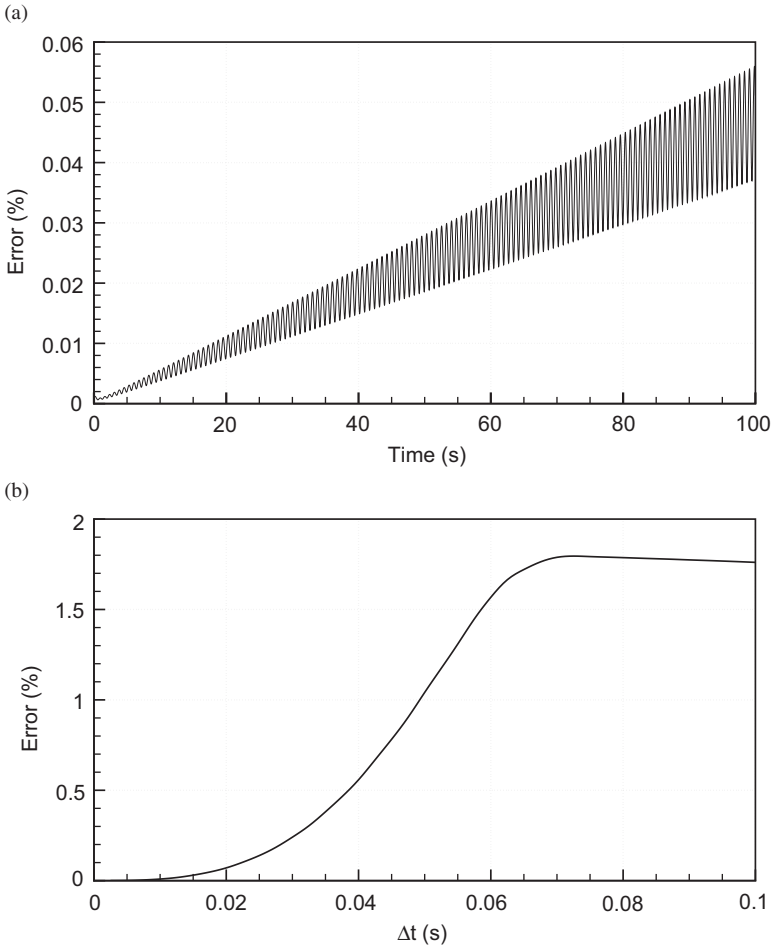

Fig. 6. Differences between analytical and numerical solutions of the linear system of equations: (a) for constant time steps $\Delta t = 0.01$ s, (b) for varying time step Δt from 0.0001 to 0.1 s.

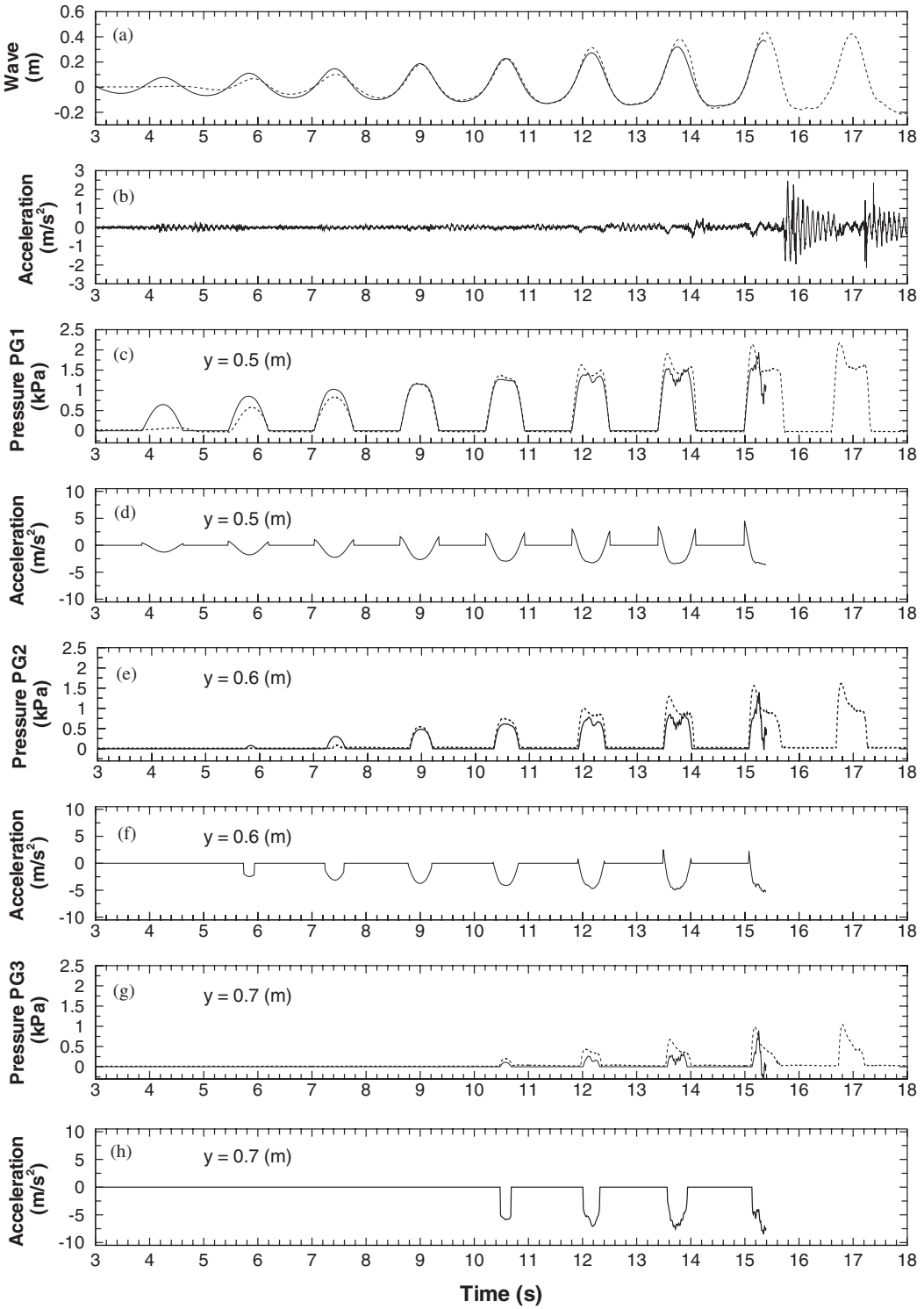

Fig. 7. Comparison of the experimental results (solid line) and theoretical calculation (dashed line) for the recording of $\lambda/2 = 1.51$ m: (a) wave elevation on the vertical plate, (b) acceleration at the top of the vertical plate; pressure in the fluid on the vertical plate at the, (c) 0.5 m, (e) 0.6 m, and (g) 0.7 m levels; acceleration in the fluid at the (d) 0.5 m, (f) 0.6 m, and (h) 0.7 m levels.

system of equations demonstrate that the proposed algorithm is stable and does not generate constantly-increasing numerical errors.

4. Results and discussion

The numerical procedures presented in Section 3 were adopted to compute growing standing waves. Calculations were made with wave parameters from the laboratory experiment (see Table 1). The potential function (2) and Eq. (5) represented by calculated coefficients b_0, c_0, b_n, c_n completely describe velocity and pressure fields in the fluid and the free surface elevation. The pressures can be calculated by Bernoulli's theorem including the movement of the wave generator in terms of dimensionless quantities as

$$-p = \tfrac{1}{2}(\phi_{,x} + \phi_{,y}) - x_g(t)\,\phi_{,y} + \omega\,\phi_{,t} + y \tag{33}$$

and the vertical acceleration in the fluid by the following total derivative:

$$a_y = \phi_{,yt} + \phi_{,y}\phi_{,yy}. \tag{34}$$

In numerical calculations, 10 components of the coefficients were used. Higher numbers of components do not provide significant improvements of fluid hydrodynamic descriptions (e.g., free surface elevation, pressures, and accelerations) and significantly increases the time of calculation. Time step Δt for each of the experiments was chosen to cover the period of the last, highest harmonic with a minimum of 10 points. Therefore, in performed numerical simulations the time steps $\Delta t = 0.009$ s was chosen.

The calculation procedure applied is well defined in space, but does not have any restraints in the time domain. To keep the same order of the solution in time as was assumed in space, the standard form of Kalman filtration was applied to the highest frequencies that appear in the calculated coefficients b_n and c_n. The proposed filtration can be considered as a way of carrying energy away from the system, because our theoretical formulation does not include dissipation. At this point, it is worth noting that the filtration method preserves the shapes of the amplitudes of the harmonics that are changing in time, and only removes signals with unwanted higher frequencies. A detailed explanation of the proposed method is well presented in Kalman's (1960) original work, whereas various practical applications are described by Wilde and Kozakiewicz (1993).

The condition of zero pressure should be satisfied at the water surface based on the dynamic free surface boundary condition. However, it does not become null, and there are residual pressures at the water surface due to the influence of the higher order terms neglected in these calculations. These nonzero pressures have been corrected in proportion to the pressure distribution curve proposed by Goda (1967). Comparable analysis of theoretical calculations and laboratory experiments is reported in Figs. 7 and 8. As examples, two different wavelengths were chosen ($\lambda/2 = 1.51$ and 1.88 m). The solid lines represent model simulation, and the dashed lines, laboratory experiments. The calculated wave data show good agreement with the experiment (Figs. 7(a) and 8(a)). The calculated and measured pressures recorded at three different levels (0.5, 0.6, and 0.7 m from the bottom) on the vertical wall in time reveal how the growing standing wave process reaches instability. As wave amplitude increases, the time history of pressures in front of the wall begins to show double humps. Just before losing stability of the wave, the second hump disappears, and an increasing value is observed in the acceleration gauge mounted on top of the wall. The moment when some part of the water breaks continuity and falls down, it creates a shock impulse as shown by the acceleration gauge in Figs. 7(b) and 8(b), and by the photograph presented in Fig. 4(f). The instability phenomenon occurs when accelerations in the fluid are close to gravity. This is clearly seen in calculated accelerations at the 0.7 m level under the wave crest (see Figs. 7(h) and 8(h)). For example, maximum acceleration in the fluid was localized under the first hump of pressure at time $t = 15.23$ s (Fig. 7(h)), and at time $t = 28.14$ s (Fig. 8(h)), with values close to the acceleration due to gravity causing loss of stability of the standing wave. Moreover, the numerical algorithm in this region passes the assumed level of convergence and also achieves the state of instability.

It is noteworthy that components with higher frequencies play a significant role in this process. They are constantly growing, and in the final phase, lead to instability of the numerical scheme. The phenomenon associated with disappearance of the second hump in the pressure records, culminating in wave breaking in front of the vertical wall, is in agreement with the earlier experimental work of Goda (1972). Fig. 9 shows the free surface shape at various times from $t = 1.13$ to 15.39 s. As time increases, the crests heighten and steepen, and the troughs correspondingly broaden. During simulations in the middle of the wavelength, the characteristic small hump appears. This nonlinear effect was also visible in the laboratory experiment (Fig. 4(d)). A similar phenomenon, but on an smaller scale, was reported by Mercer and Roberts (1992, 1994) in their steady-state solution.

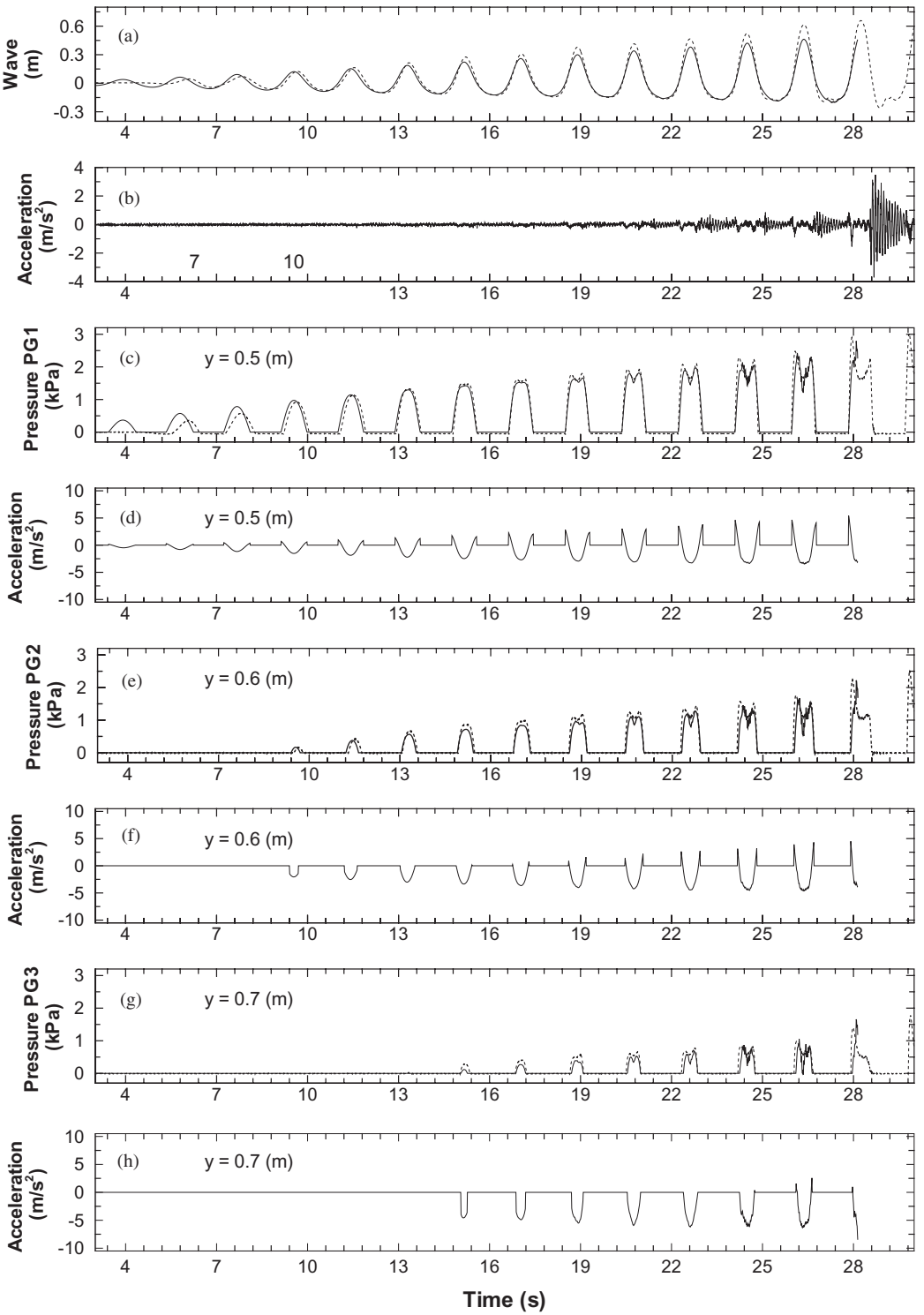

Fig. 8. Comparison of the experimental results (solid line) and theoretical calculation (dashed line) for the recording of $\lambda/2 = 1.88$ m: (a) wave elevation on the vertical plate; (b) acceleration at the top of the vertical plate; pressure in the fluid on the vertical plate at the (c) 0.5 m, (e) 0.6 m, and (g) 0.7 m levels; acceleration in the fluid at the (d) 0.5 m, (f) 0.6 m, and (h) 0.7 m levels.

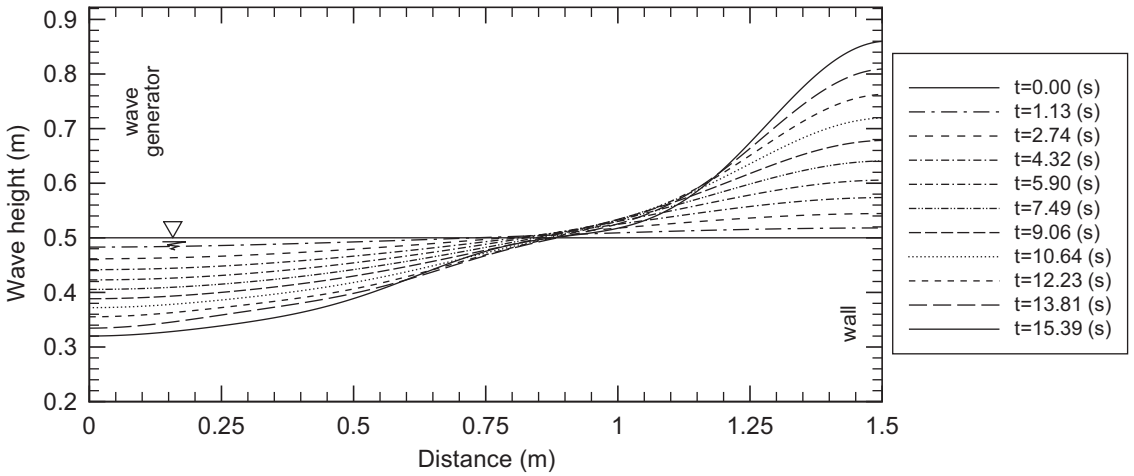

Fig. 9. Profile of waves in several time steps for the recording of $\lambda/2 = 151$ m, when the wave crest is on the vertical wall.

The present analysis demonstrates that the standing waves in the front of a wall for a medium water depth condition could lead to wave instability, and as a consequence, create a shock impact that initiates the vibrations of the structure. The simplified laboratory and numerical model gives an idea of how similar phenomena could occur in natural environments (e.g., at Gdańsk North Port). 3-D space and wave randomness are conditions that have to be considered to build more realistic models describing the instability of standing waves in front of a breakwater.

5. Conclusions

The laboratory investigation and numerical simulation reported here have yielded the following findings:

1. The amplification of standing waves in mean water depth in front of a vertical wall can lead to wave instability that results in separation of the water from the wave crest and creates an impulse-like impact.
2. The suggested method of analysis is based on a nonstationary, growing, standing wave amplitude caused by the resonance condition created by the small movement of a wave paddle generator in a limited fluid area. Vibrations of the vertical wall are used as the determinant of the moment when the wave loses stability.
3. Numerical simulations show that under the process of constantly-growing standing waves the influence of higher frequency harmonics increases with time and leads to algorithm instability.
4. The finite amplitude standing wave phenomenon, revealed by the formation of two peaks in the pressure field on the wall, was reproduced by laboratory experiments and numerical simulation. However, the mechanism presented for breaking standing waves, observed in experiments, requires more modelling efforts to be fully described.

Acknowledgements

The author dedicates this article to the memory of Prof. P. Wilde (May 19, 1931–January 12, 2006) of the Institute of Hydroengineering in Gdańsk, for his many years of continuous support and fruitful discussions, and thanks Prof. E. Thornton of the Naval Postgraduate School in Monterey for his helpful comments.

Appendix A. Definition of some functions in Section 3

The global definition of used functions used in Section 3 are as follows:

$$F(x, y, r, r+1, b_0, b_1, \ldots, b_n, c_1, \ldots, c_n)$$
$$= \frac{1}{2}\left\{\phi_{0,x}(r+1, r) - \sum_{n=1}^{N}[b_{n2}(r+1, r)G(n, r+1, r)\cosh(G_y(n, r+1, r))\sin(G_x(n, r+1, r))]\right\}^2$$

$$
\begin{aligned}
&+\frac{1}{2}\left\{\phi_{0,y}(r+1,r)+\sum_{n=1}^{N}[b_{n2}(r+1,r)G(n,r+1,r)\sinh(G_y(n,r+1,r))\cos(G_x(n,r+1,r))]\right\}^2\\
&+\omega\left\{-\dot{x}_g(r+1,r)\left[\phi_{0,x}(r+1,r)-\sum_{n=1}^{N}[b_{n2}(r+1,r)G(n,r+1,r)\cosh(G_y(n,r+1,r))\sin(G_x(n,r+1,r))]\right]\right.\\
&+\phi_{0,t}(r+1,r)+b_{0,t}(r+1,r)\\
&-\dot{x}_g(r+1,r)\sum_{n=1}^{N}[b_{n2}(r+1,r)G_{2x}(n,r+1,r)\sin(G_x(n,r+1,r))\cosh(G_y(n,r+1,r))]\\
&\left.+\dot{x}_g(r+1,r)\sum_{n=1}^{N}[b_{n2}(r+1,r)G_{2y}(n,r+1,r)\cos(G_x(n,r+1,r))\sinh(G_y(n,r+1,r))]\right\}+y,
\end{aligned}
\tag{A.1}
$$

$$
\begin{aligned}
&F_1(x,r,r+1,b_1,\ldots,b_n,c_0,c_1,\ldots,c_n)\\
&=\frac{1}{2}\left\{\phi_{0,x}(r+1,r)-\sum_{n=1}^{N}[b_{n2}(r+1,r)G(n,r+1,r)\cosh(GG_y(n,r+1,r))\sin(G_x(n,r+1,r))]\right\}^2\\
&+\frac{1}{2}\left\{\phi_{0,y}(r+1,r)+\sum_{n=1}^{N}[b_{n2}(r+1,r)G(n,r+1,r)\sinh(GG_y(n,r+1,r))\cos(G_x(n,r+1,r))]\right\}^2\\
&+\omega\left\{-\dot{x}_g(r+1,r)\left[\phi_{0,x}(r+1,r)-\sum_{n=1}^{N}[b_{n2}(r+1,r)G(n,r+1,r)\cosh(GG_y(n,r+1,r))\sin(G_x(n,r+1,r))]\right.\right.\\
&\left.+\phi_{0,t}(r+1,r)+\sum_{n=1}^{N}[b_{n,t}(r+1,r)\cosh(GG_y(n,r+1,r))\cos(G_x(n,r+1,r))\right]\\
&-\dot{x}_g(r+1,r)\sum_{n=1}^{N}[b_{n2}(r+1,r)G_{2x}(n,r+1,r)\sin(G_x(n,r+1,r))\cosh(GG_y(n,r+1,r))]\\
&\left.+\dot{x}_g(r+1,r)\sum_{n=1}^{N}[b_{n2}(r+1,r)GG_{2y}(n,r+1,r)\cos(G_x(n,r+1,r))\sinh(GG_y(n,r+1,r))\right]\right\}+y_{t2}(r+1,r),
\end{aligned}
\tag{A.2}
$$

$$
\begin{aligned}
&F_2(x,k,r,r+1,b_1,\ldots,b_n,c_0,c_1,\ldots,c_n,\mathrm{sign})\\
&=-\frac{1}{2}\phi_{0,x}(r+1,r)\sin(G_x(k,r+1,r))\sinh(GG_y(k,r+1,r))\\
&+\frac{1}{4}\sum_{n=1}^{N}\{b_{n2}(r+1,r)H(k,n,r+1,r)\sin(G_x(k,r+1,r))\sin(G_x(n,r+1,r))\\
&\times\frac{1}{k^2-n^2}\left[(k+n)\sinh(GG_y(k-n,r+1,r))+(k-n)\sinh(GG_y(k+n,r+1,r))\right]\}\\
&-\frac{1}{4}\sum_{n=1}^{N}\left\{b_{n2}(r+1,r)H(k,n,r+1,r)\cos(G_x(k,r+1,r))\cos(G_x(n,r+1,r))\right.\\
&\times\frac{1}{k^2-n^2}\left[(k+n)\sinh(GG_y(k-n,r+1,r))-(k-n)\sinh(GG_y(k+n,r+1,r))\right]\Big\}\\
&+\omega\left\{\dot{x}_g(r+1,r)\cos(G_x(k,r+1,r))\cosh(GG_y(k,r+1,r))\frac{y_{t2}(r+1,r)}{L_{t2}(r+1,r)}\right.\\
&-\dot{x}_g(r+1,r)\cos(G_x(k,r+1,r))\sinh(GG_y(k,r+1,r))\frac{1}{k\pi}\\
&+\dot{x}_g(r+1,r)\sin(G_x(k,r+1,r))\sinh(GG_y(k,r+1,r))\left[\frac{1}{2}-\frac{x}{2L_{t2}(r+1,r)}\right]\\
&\left.+\mathrm{sign}\frac{L_{t2}(r+1,r)}{\Delta tk\pi}\cos(G_x(k,r+1,r))\sinh(GG_y(k,r+1,r))\right\}
\end{aligned}
\tag{A.3}
$$

$$
\begin{aligned}
&F_3(x,k,r,r+1,b_1,\ldots,b_n,c_0,c_1,\ldots,c_n)\\
&=\frac{1}{4}b_{n2}(r+1,r)[G(k,r+1,r)]^2 y_{2t}(r+1,r)\left[\sin^2(G_x(k,r+1,r)-\cos^2(G_x(k,r+1,r))\right]\\
&\quad+\frac{1}{8}b_{n2}(r+1,r)G(k,r+1,r)\sinh(2GG_y(k,r+1,r))\left[\sin^2(G_x(k,r+1,r)+\cos^2(G_x(k,r+1,r))\right]
\end{aligned}
\tag{A.4}
$$

were the internal functions are:

(a) the velocity of the wave generator paddle:

$$
\dot{x}_g(r+1,r)=\frac{x_g(r+1)-x_g(r)}{\Delta t},
\tag{A.5}
$$

(b) the acceleration of the wave generator paddle:

$$
x_g(r+1,r)=\frac{\ddot{x}_g(r+2)-x_g(r+1)-x_g(r)+x_g(r-1)}{2\Delta t^2},
\tag{A.6}
$$

(c) the differential of the potential function ϕ_0 (x,y,t):

$$
\begin{aligned}
&\phi_{0,x}(r+1,r)=\dot{x}_g(r+1,r)\left[1-\frac{x}{L_{t2}(r+1,r)}\right],\\
&\phi_{0,y}(r+1,r)=\dot{x}_g(r+1,r)\frac{y}{L_{t2}(r+1,r)},\\
&\phi_{0,t}(r+1,r)=\omega\ddot{x}_g(r+1,r)\left[x-\frac{x^2-y^2}{2L_{t2}(r+1,r)}\right]-(\dot{x}_g(r+1,r))^2\frac{x^2-y^2}{2L_{t2}^2(r+1,r)},
\end{aligned}
\tag{A.7}
$$

(d) the differential of the parameter:

$$
b_{0,t}(r+1,r)=\frac{b_0(r+1)-b_0(r)}{\Delta t},
\tag{A.8}
$$

(e) and some additional relations, as follows:

$$
\begin{aligned}
b_{n2}(r+1,r)&=\frac{b_n(r+1)+b_n(r)}{2},\\
G(n,r+1,r)&=\frac{n\pi}{L_{t2}(r+1,r)}, \qquad H(k,n,r+1,r)=\frac{kn\pi}{L_{t2}(r+1,r)},\\
G_x(n,r+1,r)&=\frac{n\pi x}{L_{t2}(r+1,r)}, \qquad G_{2x}(n,r+1,r)=\frac{n\pi x}{L_{t2}^2(r+1,r)},\\
G_y(n,r+1,r)&=\frac{n\pi y}{L_{t2}(r+1,r)}, \qquad G_{2y}(n,r+1,r)=\frac{n\pi y}{L_{t2}^2(r+1,r)},\\
GG_y(n,r+1,r)&=\frac{n\pi y_{t2}(r+1,r)}{L_{t2}(r+1,r)}, \qquad GG_{2y}(n,r+1,r)=\frac{n\pi y_{t2}(r+1,r)}{L_{t2}^2(r+1,r)}.
\end{aligned}
\tag{A.9}
$$

References

Amick, C.J., Toland, J.F., 1987. The semi-analytic theory of standing waves. Philosophical Transactions of the Royal Society of London, Series A 411, 123–137.

Broyden, C., 1965. A class of methods for solving nonlinear simultaneous equations. Mathematics of Computation 19, 577–593.

Bruun, P., 1986. Port Engineering, Vol. I. Gulf Publishing Company, Houston

CEM, 2001. Coastal Engineering Manual. US Army Corps of Engineers, Washington, DC.

Cooker, M.J., Peregrine, D.H., 1990a. A model for breaking wave impact pressures. In: Proceedings of the 22nd ASCE Coastal Engineering Conference, Delft, The Netherlands, pp. 1473–1486.

Cooker, M.J., Peregrine, D.H., 1990b. Violent water motion at breaking-wave impact. In: Proceedings of 22nd ASCE Coastal Engineering Conference, Delft, Netherlands, pp. 164–176.
Cooker, M.J., Peregrine, D.H., 1992. Wave impact pressure and its effect upon bodies lying on the sea bed. Coastal Engineering 18, 205–229.
Cooker, M.J., Peregrine, D.H., 1995. Pressure–impulse theory for liquid impact problems. Journal of Fluid Mechanics 297, 193–214.
Danel, P., 1952. On the limiting clapotis—gravity waves. National Bureau of Standards Circular 521, 35–38.
Dean, R.G., Dalrymple, R.T., 1984. Water Wave Mechanics for Engineers and Scientists. Advanced Series on Ocean Engineering, Vol. 2. World Scientific, Singapore.
Fenton, J.D., 1985. Wave forces on vertical walls. ASCE Journal of Waterway, Port, Coastal and Ocean Engineering 111 (4), 693–718.
Fultz, D., 1962. An experimental note on finite-amplitude standing gravity waves. Journal of Fluid Mechanics 13, 193–212.
Goda, Y., 1967. The fourth order approximation to the pressure of standing waves. Coastal Engineering in Japan 10, 1–11.
Goda, Y., 1972. Experiments on the transition from nonbreaking to postbreaking wave pressures. Coastal Engineering in Japan 15, 81–90.
Goda, Y., 1985. Random Seas and Design of Maritime Structures. University of Tokyo Press, Tokyo, Japan.
Hueckel, S., 1976. Stability and scour hazard problems of a vertical breakwater loading by water waves. Archive of Hydrotechnics 23, 1–14 (in Polish).
Iwagaki, Y., Sakai, T., Asano, T., Mase, H., Koseki, M., 1980. Experimental study on pressures due to irregular standing waves. Coastal Engineering in Japan 23, 121–129.
Iwata, K., Kiyono, H., 1985. Breaking of standing two-components composite and irregular waves. Coastal Engineering in Japan 28, 71–87.
Jeng, D.S., 2002. Wave kinematics of partial reflection from a vertical wall. Ocean Engineering 29, 1711–1724 Technical Note.
Kalman, R.E., 1960. A new approach to linear filtering and prediction problems. ASME Journal of Basic Engineering 82-D, 35–45.
Kishi, T., 1959. The possible highest gravity waves in shallow water. Coastal Engineering in Japan 2, 9–16.
Kjeldsen, S.P., 1981. Shock pressures from deep water breaking waves. In: Proceedings of the International Symposium on Hydrodynamics in Ocean Engineering, Trondheim, Norway, pp. 567–584.
Lappo, D.D., Zagryadskaya, N.N., 1977. Studies of pressure and energy of standing waves. ASCE Journal of Waterway, Port, Coastal and Ocean Engineering 103 (3), 335–347.
Le Méhauté, B., 1976. An Introduction to Hydrodynamics and Water Waves. Springer, New York.
Longuet-Higgins, M.S., 2001. Vertical jets from standing waves. Philosophical Transactions of the Royal Society of London, Series A 457, 495–510.
Longuet-Higgins, M.S., Drazen, D.A., 2002. On steep gravity waves meeting a vertical wall: a triple instability. Journal of Fluid Mechanics 457, 2137–2149.
Luke, I.C., 1967. A variational principle for a fluid with a free surface. Journal of Fluid Mechanics 27, 395–397.
Lundgren, H., 1969. Wave shock forces: an analysis of deformations and forces in the wave and in the foundation. In: Proceedings of the Symposium on Research on Wave Action, Vol. II, Paper 4, Delft, The Netherlands.
Mercer, G.N., Roberts, A.J., 1992. Standing waves in deep water: their stability and extreme form. Physics of Fluids A 4, 259–269.
Mercer, G.N., Roberts, A.J., 1994. The form of standing waves on finit depth water. Wave Motion 19, 233–244.
Miche, R., 1944. Mouvement ondulatoire de la mer en profondeur constante ou decroissante. Annales Ponts et Chaussées 121, 285–318 (in French).
Nagai, S., 1968. Pressures of partial standing waves. ASCE Journal of Waterways and Harbors Division 94 (3), 273–286.
Nagai, S., 1969. Pressures of standing waves on vertical wall. ASCE Journal of Waterways and Harbors Division 95 (1), 53–76.
Oumeraci, H., Klammer, P., Partenscky, H.W., 1993. Classification of breaking wave loads on vertical structures. ASCE Journal of Waterway, Port, Coastal and Ocean Engineering 119 (4), 381–397.
Oumeraci, H., Partenscky, H.W., Kohlhase, S., Klammer, P., 1992. Impact loading and dynamic response of caisson breakwaters. Results of large-scale model tests. In: Proceedings of 23rd ASCE Coastal Engineering Conference, Venice, Italy, pp. 1475–1488.
Oumeraci, H., Kortenhaus, A., Allsop, W., de Groot, M., Crouch, R., Vrijling, H., Voortman, H., 2001. Probabilistic Design Tools for Vertical Breakwaters. Balkema Publishers, The Netherlands.
Penney, W.G., Price, A.T., 1952. Finite periodic stationary gravity waves in a perfect liquid. Philosophical Transactions of the Royal Society of London, Series A 244, 254–284.
Press, W.H., Teukolsky, S.A., Vetterling, W.T., Flannery, B.P., 1992. Numerical Recipes in Fortran 77. Cambridge University Press, New York, USA.
Rayleigh, L., 1915. Deep water waves, progressive or stationary, to the third order of approximation. Philosophical Transactions of the Royal Society of London, Series A 91, 345–353.
Richert, G., 1974. Shock pressures of breaking waves. Hydraulic Laboratory Bulletin No. 84. Royal Institute of Technology, Stockholm, Sweden.
Romańczyk, W., 1992a. Mathematical model for free vibrations of structures due to wave loading. Hydrotechnical Transactions 55, 231–244.
Romańczyk, W., 1992b. Measurements and analysis of wave loads on the breakwater in Gdańsk North Port. Application of Mechanics in Civil Engineering, IBW PAN, Gdańsk, Poland, pp. 97–109.
Romańczyk, W., 1994. Vibrations of vertical elastically supported plate loaded by standing breaking waves. Ph.D. Thesis, Institute of Hydroengineering of Polish Academy of Sciences, Poland (in Polish).

Romańczyk, W., Sobierajski, E., 1994. Vibration of the North Harbour breakwater due to wave impact. In: National Symposium of Maritime Engineering and Environment. IBW PAN, Gdańsk, Poland, pp. 103–110 (in Polish).

Rundgren, L., 1958. Water wave forces—a theoretical and laboratory study. Hydraulic Laboratory Bulletin No. 54. Royal Institute of Technology, Stockholm, Sweden.

Sainflou, G., 1928. Essai sur les digues maritimes verticales. Annales Ponts et Chaussées 98 (4), 5-48 (in French).

Schultz, W.W., Vanden-Broeck, J.M., Jiand, L., Perlin, M., 1998. Highly nonlinear standing water waves with small capillary effect. Journal of Fluid Mechanics 396, 253–272.

Schwartz, L.W., Whitney, A.K., 1981. A semi-analytic solution for nonlinear standing waves in deep water. Journal of Fluid Mechanics 107, 147–171.

Sobierajski, E., 1992. The Marine Harbour Laboratory of the Institute of Hydroengineering in Gdańsk. Application of Mechanics in Civil Engineering, IBW PAN, Gdańsk, Poland, pp. 131–136 (in Polish).

Tadjbakhsh, I., Keller, J.B., 1960. Standing surface waves of finite amplitude. Journal of Fluid Mechanics 8, 442–451.

Tsai, C.P., Jeng, D.S., 1994. Numerical Fourier solutions of standing waves in finite water depth. Applied Ocean Research 16, 185–193.

Vanden-Broeck, J.M., 1984. Nonlinear gravity-capillary standing waves of arbitrary uniform depth. Journal of Fluid Mechanics 139, 97–104.

Vinje, T., Brevig, P., 1981. Numerical calculations of forces from breaking waves. In: Proceedings of the International Symposium on Hydrodynamics in Ocean Engineering. Trondheim, Norway, pp. 547–567.

Wiegel, R.L., 1964. Oceanographical Engineering. Prentice-Hall Inc., Englewood Cliffs, NJ.

Wilde, P., Kozakiewicz, A., 1993. Kalman Filter Method in the Analysis of Vibrations due toWater Waves. Advanced Series on Ocean Engineering, Vol. 6. World Scientific, Singapore.

Wood, D.J., Peregrine, D.H., 1998. Two and three-dimensional pressure–impulse models of wave impact on structures. In: Proceedings of 26th ASCE Coastal Engineering Conference. Copenhagen, Denmark, pp. 1502–1515.

Wood, D.J., Peregrine, D.H., 2000. Study of wave impact against a wall with pressure–impulse theory: Part 1, traped air. ASCE Journal of the Waterway Port Coastal and Ocean Division 126, 182–190.